In this issue

European Centre for Medium-Range Weather Forecasts

Shinfield Park, Reading, Berkshire RG2 9AX, UK

Fax: . . . . . .+44 118 986 9450

Telephone: National 0118 949 9000

International . . . . . .+44 118 949 9000

Public Web site . . . . . .http://www.ecmwf.int

Member States' Web site . . . . . .http://wms.ecmwf.int

ACCESS TO ECMWF'S MEMBER STATES WEB SERVICES

A facilitated access to the ECMWF's Member States Web services (http://wms.ecmwf.int) has been implemented. Users from the Member States' and Co-operating States' meteorological services are recognised by their domain address and allowed to access most parts of the website without any further specific system. This includes, in particular, access to all forecast and verification products. Wherever possible, a link from Member States' Intranet will be implemented. Some areas, such as archive retrieval or computer access, still need a specific access control device such as SecurID or certificate.

Front Cover

Virtual tour of MARS on the Web.

Editorial

Roberto Buizza, David Richardson and Tim Palmer describe the new high-resolution ensemble prediction system on page 2. Tests of the new system have indicated that it provides a gain in predictability in the Northern Hemisphere of about 12 hours, compared with the previous ensemble system. This goes a considerable way towards meeting the objectives set out in the ten-year (1999-2008) Strategic Plan adopted by Council in June 1999. The new high-resolution system outperforms a "poor man's" ensemble containing higher-resolution operational models from different Centres and it offers considerable benefits for users.

On page 9 Baudouin Raoult gives a step-by-step guide to accessing the MARS archival system using a standard web browser. Readers of the Newsletter are encouraged to try out the new facility, using the article as a guide to navigating through the principal stages of exploring the components of the system. On page 17 Anton Beljaars, Christian Jacob and Jean-Jacques Morcrette describe several additional fields that are now produced routinely by the post-processing system and stored in MARS. The new fields (10m wind gusts, subgrid stratiform precipitation fraction, boundary-layer height, and net clear-sky radiation at the top of the atmosphere and at the surface) are likely to be particularly useful to users of the Centre's forecasts. ❑

Changes to the Operational Forecasting System

The computation of the EPS stochastic physics tendencies was corrected on 15 December 2000. This removed a feature introduced with cycle 21r2 (July 1999) which has occasionally produced non-realistic values for some EPS members (notably for near-surface temperature and humidity).

Due to the failure of the ERS-2 navigation instruments, both the ambiguous surface winds and the altimeter data became unavailable on 17 January 2001

The amplitude of the EPS initial perturbations was upscaled by a factor two on 5 February 2001. This rescaling was linked to the data-assimilation changes introduced with cycle 22r3 in June 2000 which resulted in a lack of spread.

The ERS-2 altimeter data were switched on again in the oceanic-waves data assimilation on 6 March 2001. The ERS-2 winds remain unavailable.

Future changes

Testing of cycle 23r4 is going on. This new cycle allows more and better uses of satellite data over land and sea ice. It also contains a minor change to the horizontal diffusion and provides more frequent calls to the radiation code in the data assimilation. ❑

François Lalaurette

The new 80-km High-Resolution ECMWF EPS

Small errors in initial conditions (initial uncertainties) and the approximate representation of atmospheric processes in numerical models (model uncertainties) are the two main sources of forecast error. These two sources of uncertainty limit the skill of single, deterministic forecasts in a highly flow-dependent way, with days of high quality forecasts followed by days of poor quality forecasts.

A complete description of the weather prediction problem can be stated in terms of the time evolution of an appropriate probability density function (PDF) in the atmosphere's phase space. Ensemble prediction based on a sampling of this PDF by a finite number of deterministic integrations designed to represent both initial and model uncertainties appears to be the only feasible method to predict the PDF beyond the range of linear error growth (Fig. 1).

Routine real-time execution of the ECMWF EPS started in December 1992 with a 33-member T63L19 configuration (spectral triangular truncation T63 and 19 vertical levels, *Palmer et al.* 1993, *Molteni et al.* 1996). This first version of the EPS simulated initial uncertainties due to errors growing in the forecast time (*Buizza & Palmer* 1995) but did not simulate model uncertainty. A major upgrade to a 51-member T_L159L31 system (spectral triangular truncation T159 with linear grid) took place in 1996 (*Buizza et al.* 1998). Two further important modifications were introduced in 1998. In March 1998, initial uncertainties due to

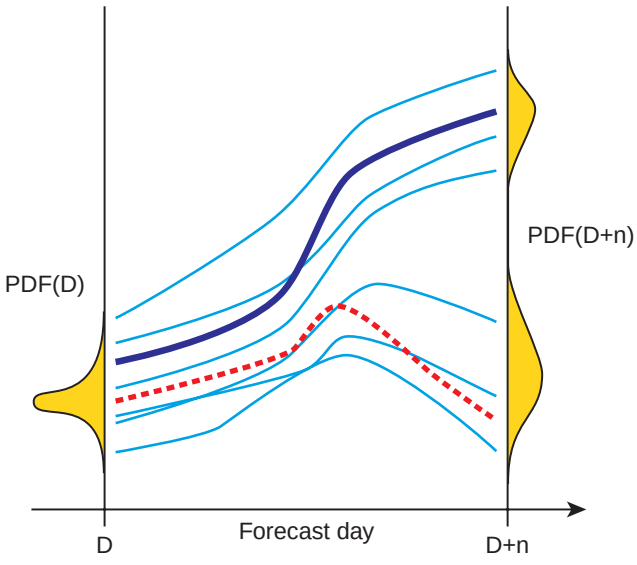

Figure 1 Schematic of ensemble prediction. The initial probability PDF(D) represents the initial uncertainties. From the best estimate of the initial state a single deterministic forecast (bold blue solid curve) is performed. This single deterministic forecast fails to predict correctly the future state (red dotted curve). An ensemble of perturbed forecasts (thin blue solid curves) starting from perturbed initial conditions designed to sample the initial uncertainties can be used to estimate the probability PDF(D+n) at the future time D+n.

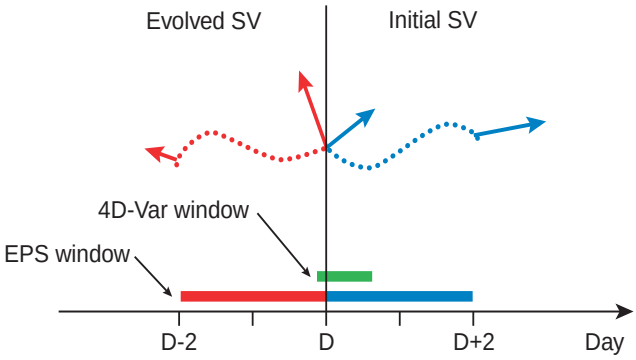

Figure 2 The initial perturbations of the EPS starting at day D are defined to sample perturbations growing in the past, between days (D–2) and D, and in the future, between days D and (D+2). The first set of perturbations (red arrows), are defined by using singular vectors evolved from day (D–2) to day D, while the second set of perturbations (blue arrows) are defined by using initial singular vectors. With this choice, the time-interval spanned by the two sets of singular vectors cover the time-interval spanned by the 4D-Var data-assimilation procedure (green). NH – summer (30 cases) NH – winter (57 cases)

perturbations that had grown during the data assimilation system (evolved singular vectors, *Barkmeijer et al.* (1999)) were added to the initial uncertainties due to errors growing rapidly in the forecast time (initial singular vectors). Figure 2 is a schematic of the way the ensemble initial perturbations have been defined since March 1998. The initial perturbations of the ensemble starting at day D are defined by combining the singular vectors growing between day D-2 and day D, evolved at day D, and the singular vectors growing between day D and D+2, at initial time. In October 1998, a scheme to simulate model uncertainties due to random model error in the parametrized physical processes was introduced (*Buizza et al.* 1999).

The changes introduced in 1996 and 1998 improved the performance of the EPS (*Buizza et al.* 2000). Compared to the initial 33*T63L19 system, the upgraded 51*T_L159L31 system had a better level of spread (both in terms of anomaly correlation and root-mean-square distance), a more skilful ensemble-mean, a higher chance of including the verification analysis inside the forecast range, and more accurate probabilistic predictions (as measured by different skill measures such as the Brier skill score, the area under the relative-operating-characteristic curve, the ranked-probability skill score and the potential economic value.

Long-term goals for the EPS.

The Strategic Plan 1999-2008 (adopted by the ECMWF Council in June 1999, ECMWF (1999)) states the long-term goals for deterministic forecasting and ensemble prediction:

Deterministic Forecasting: A robust measure of the performance of the Centre's deterministic forecasts is the forecast range for which the anomaly correlation of the

Northern Hemisphere 500hPa height field exceeds the 60% level. A realistic 10-year target is to extend this forecast range by one day.

Ensemble Prediction: Brier-skill-scores for probabilistic forecasts are the appropriate measure of performance of the EPS. Here the historical record is too short to be helpful in formulating targets. However, in line with the first goal, a reasonable target is a gain of one day at D+6 in the Brier-skill-score for probabilistic forecasts of moderate 850hPa temperature anomalies (4K or larger) in Europe.

This strategic plan defines the goals that any modifications of the EPS should aim to achieve in the 10-year period from 1999. It is the intention of this work to document whether a recent increase of the EPS resolution had made achievement of the long-term strategic targets closer.

The new 80-km High-resolution EPS

Following extensive experimentation, the resolution of the ECMWF analysis and forecasting system was increased on 21 November 2000:

- Deterministic model and analysis: from $T_L319L60$ (60 km grid-point spacing) to $T_L511L60$ (40 km grid-point spacing);
- EPS: from T_L159 (120km grid-point spacing) to T_L255 (80km grid-point spacing).

Thus, compared to the EPS the new 80-km High Resolution EPS (HEPS) is run with a finer horizontal resolution and starting from a higher-resolution analysis.

This report documents the impact of the increased resolution on the accuracy of the ECMWF ensemble system. To limit the number of figures and tables, and following the strategic goals, only 850 hPa temperature fields are considered. For each ensemble configuration, the following measures of ensemble performance (hereafter called 'scores') have been considered:

- Skill of the EPS control, measured in terms of anomaly-correlation coefficient (ACC);
- Ensemble spread with respect to the control forecast, measured in terms of ACC;
- Skill of the ensemble-mean, measured in terms of ACC;
- Brier skill score (BSS) of EPS probabilistic predictions of positive and negative anomalies with amplitudes larger than the seasonal variability (defined as the standard deviation of the analysed fields).

The EPS and the HEPS configurations have been compared for 87 cases covering two periods: summer 1999 (30 cases, from 2 to 30 August) and winter 1999-2000 (57 cases, from 26 November to 27 December 1999 and from 22 January to 15 February 2000). All scores have been computed using forecast and analysed fields defined on a regular latitude-longitude grid, with a spacing of 2.5°. Scores have been computed for two regions, the Northern Hemisphere (NH) and Europe. These are shown mostly for NH, mainly for reason of space, but also because differences between the EPS and HEPS score distributions are less statistically significant for Europe.

The verifying analysis is defined by the operational $T_L319L60$ analysis, and not by the $T_L511L60$ analysis from which the HEPS starts. This choice has a negligible effect in the forecast range after forecast day 2, but it has a small but detectable impact for earlier forecast ranges when it slightly favours the EPS.

For each area and for each ensemble configuration, mean scores computed for the summer and the winter periods are shown (confidence intervals have been computed, but figures become unreadable if they are added to the average values). The degree of similarity between the distribution of scores of the two ensemble configurations is measured by the Rank-Mann-Wilcoxon (RMW) test. The RMW test estimates the probability that the distribution of scores of the EPS and the HEPS configurations are statistically distinguishable: low/high RMW values indicate that there is a small/large probability that the two distributions are subsamples of the same overall distribution. For any score, the HEPS and EPS distributions are considered statistically different if RMW≤10, that is if there is a 10% or lower probability that the two distributions of ACC scores comes from the same overall distribution.

Target skill and Relative Improvement index

To highlight the level of skill gained, compared with the long-term strategic target of a one-day improvement, the average HEPS scores are contrasted with the average EPS scores and with the average EPS scores shifted by one day (EPS(d-1)), i.e. with an EPS system characterised by a one-day gain in skill. If the skill of the HEPS lies between the skills of the EPS and the EPS(d-1) it means that HEPS is better than EPS; if the HEPS skill is equal or above the skill of EPS(d-1) it means that HEPS shows a gain in skill of one day or more.

To be able to compare the impact of the change in resolution on different scores, for any score measure, *SC*, the Relative Improvement (RI) index *RI*(*SC*)

$$RI(SC) = \frac{SC[HEPS] - SC[EPS]}{SC[EPS(d-1)] - SC[EPS]}$$

has been computed. The RI index is a normalised measured of the gain in skill obtained by configuration HEPS, with the normalisation coefficient defined by the long-term strategic target of a one-day gain. A 100% positive RI indicates an improvement equivalent to one day. Since, by construction, the EPS has been designed for forecast lengths of two days or longer, the RI has been computed only for forecast days 2 to 10.

The skill of the EPS control, the skill of the ensemble-mean, and the ensemble spread

Figure 3 shows the skill of the control forecast, the skill of the ensemble-mean and the ensemble spread. The top panels of Fig. 3 show that the skill of the HEPS control is slightly higher than the skill of the EPS control, with differences statistically significant up to forecast day 6 for summer (Fig. 3, top-left panel) and 8 for winter (Fig. 3, top-right panel). The comparison between the ACC curves of HEPS and EPS(d-1) indicates that the HEPS gain in skill is about 3-6 hours, definitely less than 12 hours. The fact that at forecast day 1 the ACC of the HEPS control is lower than the ACC of the EPS control is a direct consequence of the

choice of using the operational $T_L319L60$ verifying analysis (see comment above). The middle panels of Fig. 3 shows the ensemble spread of the two systems: the EPS spread is larger than the HEPS spread especially for the summer period (Fig. 3, left-middle panel). The bottom panels of Fig. 3 shows the skill of the ensemble-mean: apart for forecast day 1, the HEPS ensemble-mean has a higher ACC. The gain in skill induced by the increased resolution is larger for winter (Fig. 3, bottom-right panel). The RMW test shows that the differences are statistically significant for all forecast times for winter (Fig. 3, bottom-right panel) and up to forecast day 8 for summer (Fig. 3, bottom-left panel). The comparison of the HEPS and the EPS (d-1) scores indicates that that the HEPS ensemble-mean gain in skill is about 6-12 hours (Fig. 3, bottom panels), which is higher than the gain shown for the control (Fig. 3, top panels).

Brier skill score of temperature-anomaly predictions

The following two events have been considered: 'positive 850hPa temperature anomalies larger than one standard deviation' and 'negative 850hPa temperature anomalies larger than one standard deviation'. The accuracy of any probabilistic prediction of these two events have been assessed using the Brier skill score, the rank probability skill score and measures related to the Relative Operating Characteristic curve. For reasons of space, only BSS are shown, but similar conclusions could have been drawn by considering the other scores.

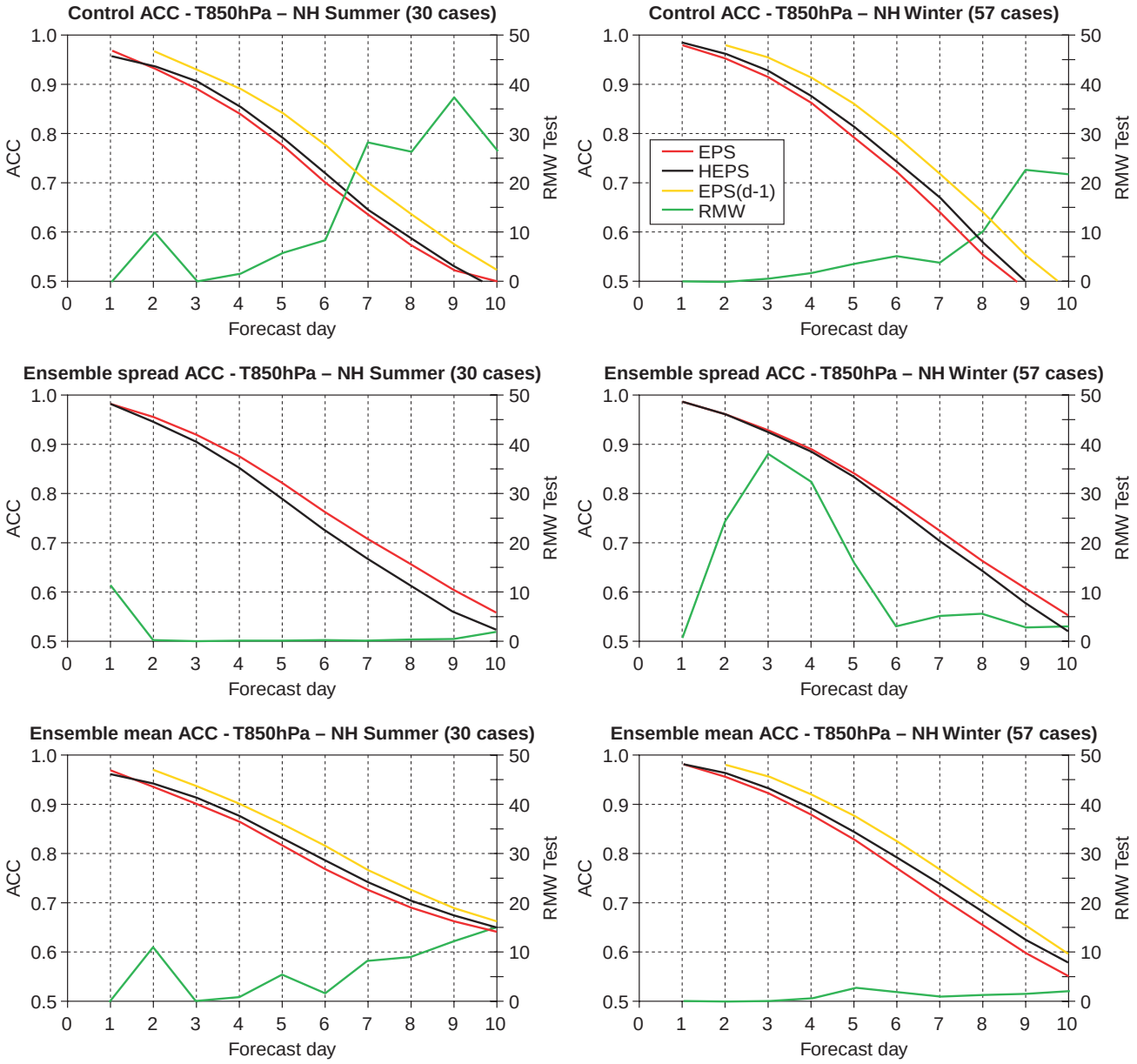

Figure 3 Top panels: mean ACC skill scores (left vertical axis) of the EPS forecasts (black curve), the HEPS forecasts (red curve) and the EPS(d-1) forecasts (yellow curve), and the Rank-Mann-Wilcoxon test value (green curve, right vertical axis) over the NH for summer (left) and winter (right). Middle panels: the ensemble spread. Bottom panels: as top panel but for the ACC skill score of the ensemble-mean. NH – summer (30 cases) NH – winter (57 cases)

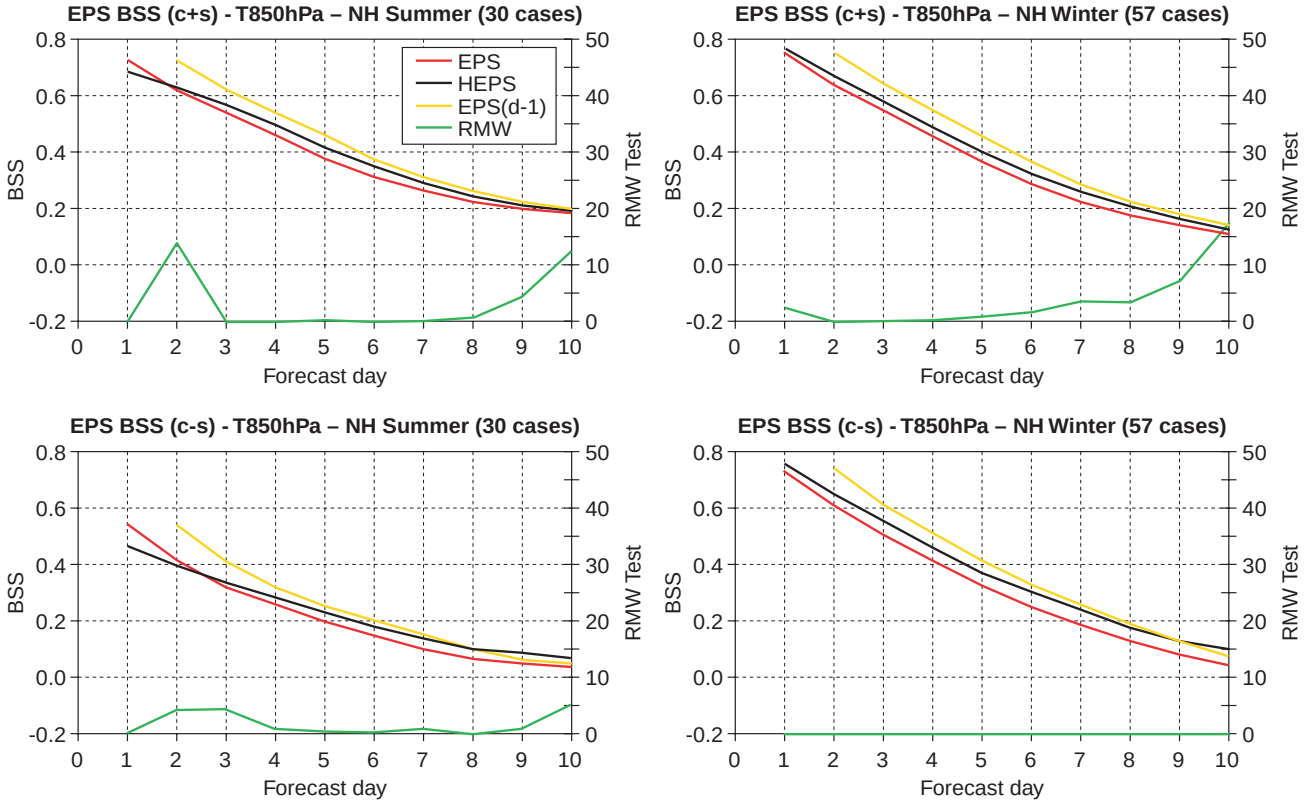

Figure 4 Top panels: The Brier skill score of the probabilistic predictions of 'positive 850hPa temperature anomalies larger than one standard deviation' (left vertical axis) for the EPS forecasts (black curve), the HEPS forecasts (red curve) and the EPS(d-1) forecasts (yellow curve), and the Rank-Mann-Wilcoxon test value (green curve, right vertical axis) over the NH for summer (left) and winter (right). Bottom panels: as top panels but for the event 'negative 850hPa temperature anomalies larger than one standard deviation'. Europe - summer (30 cases) Europe - winter (57 cases)

Figure 4 show the BSS for the three ensemble configurations, EPS, HEPS and EPS (d-1). During summer (top panels), results indicate that the HEPS performs better, with gains in predictability of 12 hours or more for forecast ranges beyond day 4 with peaks of more than 1 day at forecast days 9 and 10 for negative anomalies (Fig. 4, top-right panel). Differences between the EPS and the HEPS are significant for all forecast ranges, apart for forecast day 10 during summer (Fig. 4, top-left panel). Similar results are shown for winter (Fig. 4, bottom panels), where differences are slightly larger.

Figure 5 is similar to Fig. 4 but shows the BSSs for Europe. Compared to the NH (Fig. 4), the RMW test values for Europe indicate that the distributions of EPS and HEPS scores are less significantly different. However, the results confirm the positive impact of the resolution increase, with gains in predictability even larger than the one shown for the NH for the last forecast days.

Relative Improvement Index

Figure 6 shows the relative improvement index, RI, computed over the NH for five skill measures: the control ACC and BSS, the ensemble-mean ACC and BSS, and the EPS BSS. The results indicate that, for winter (Fig. 6, bottom panel), all the RIs are positive while, for summer (Fig. 6, top panel), the RIs are positive for all forecast days apart for some at day 2 and 10. The very small day-2 differences are due to the fact that the $T_L319L60$ analysis is used for verification (see comment above). For summer at forecast day 10, the negative RIs are the ones computed for the control forecast.

The long-term strategic goal sets a target of a one-day gain in predictability at forecast day 6 for EPS probabilistic predictions of moderate 850hPa temperature anomalies, using the BSS as a measure of skill. The results show that the RIs for EPS probabilistic predictions (Fig. 6, red bars) are between 55% and 7% for summer (Fig. 6, top) and between 45% and 66% for winter (Fig. 6, bottom) at forecast days 5 to 7.

It is interesting to compare the RIs computed for the BSS of the control (red), the ensemble-mean (cyan) and the EPS (burgundy). For all forecast steps, the RIs computed for the EPS are the largest. Differences are particularly large between the RIs computed for the EPS and the control forecast, especially at the end of the ten-day forecast range. These differences among the RIs indicate that, due to the increased resolution, the ensemble probability forecasts have improved more than categorical forecasts given by the control or the ensemble-mean forecast (this result is valid when using the BSS as accuracy measure).

Since the distributions of the scores for the EPS and HEPS are less statistically significant for Europe, relative improvement indices have not been computed for Europe. Despite this, an indication of the level of gains in predictability obtained over Europe can be gathered by looking at Fig. 5.

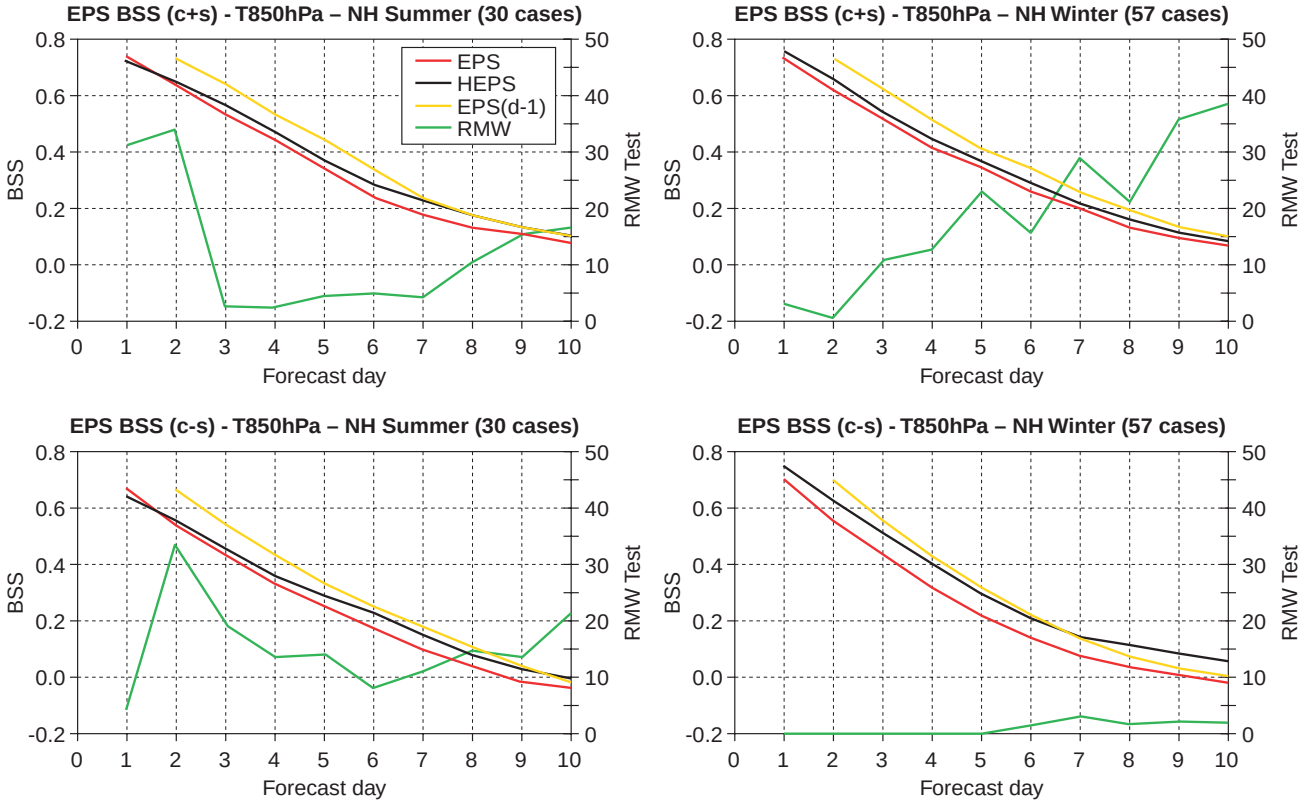

Figure 5 Top panels: The Brier skill score of the probabilistic prediction of 'positive 850hPa temperature anomalies larger than one standard deviation' (left vertical axis) for the EPS forecasts (black curve), the HEPS forecasts (red curve) and the EPS(d-1) forecasts (yellow curve), and the Rank-Mann-Wilcoxon test value (green curve, right vertical axis) over Europe for summer (left) and winter (right). Bottom panels: as top panels but for the event 'negative 850hPa temperature anomalies larger than one standard deviation'.

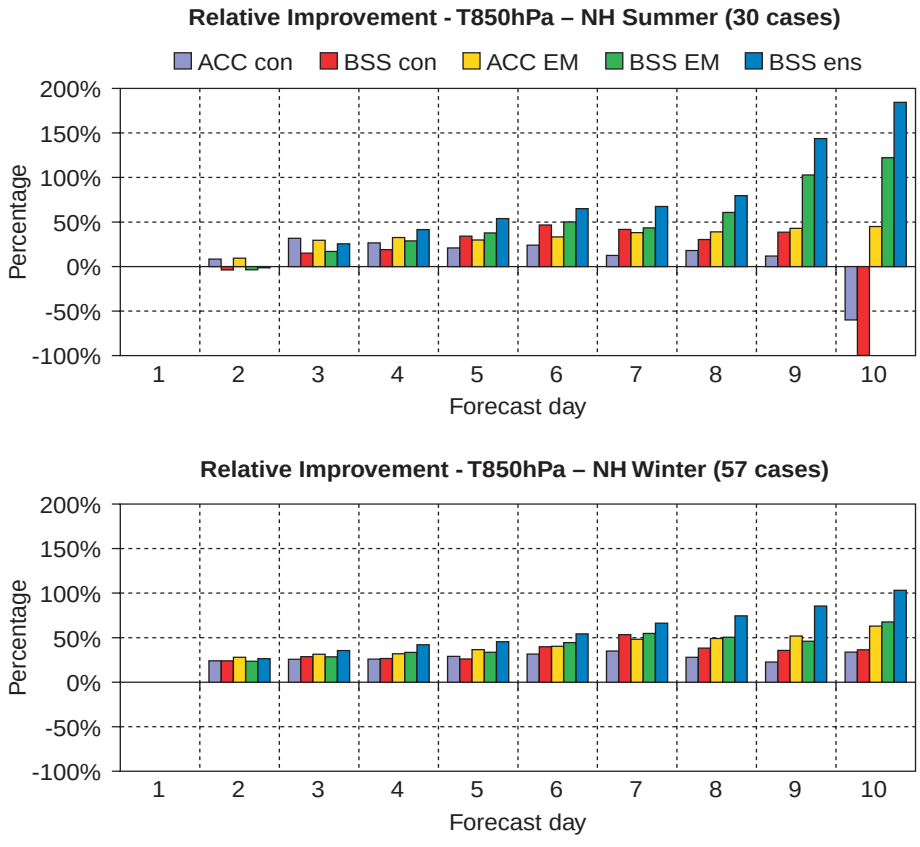

Figure 6 The Relative Improvement index (RI) for summer (top) and winter (bottom) computed over the northern hemisphere: the control ACC skill score (violet), the control Brier skill score (red), the ensemble-mean ACC skill score (yellow), the ensemble-mean Brier skill score (green) and the EPS Brier skill score (blue). A Relative Improvement of 100% indicates a gain in predictability of one day (see text for details).

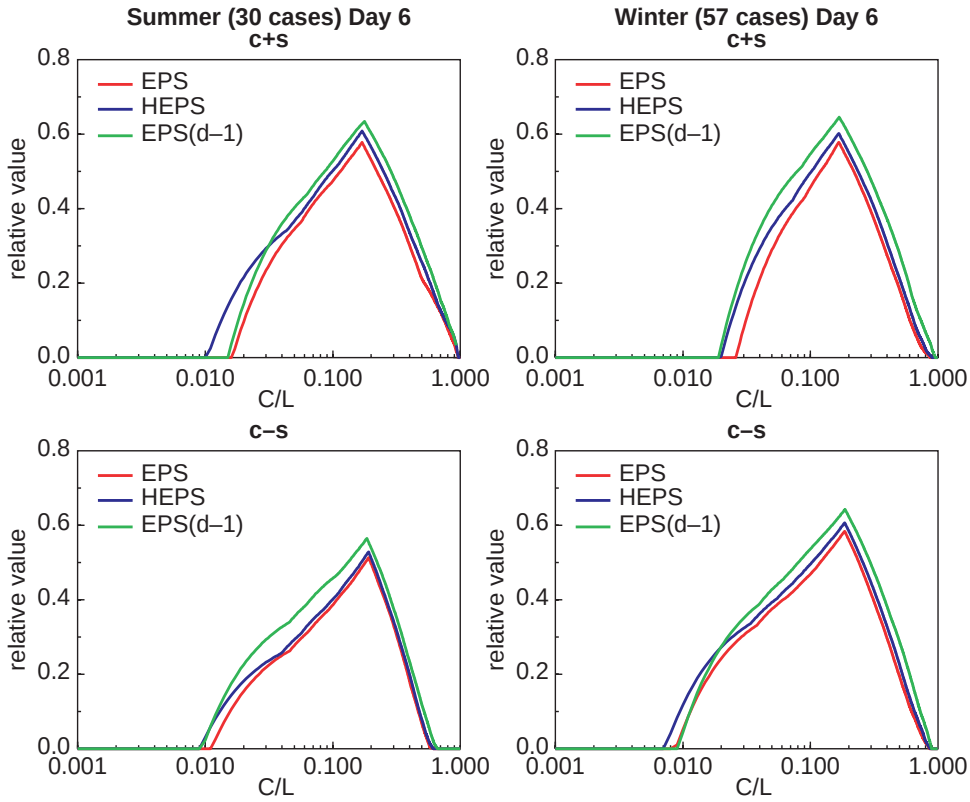

Figure 7 Value V of the EPS (red), HEPS (blue) and EPS(d–1) (green) ensemble configurations for summer (left panels) and winter (right panels) for the prediction of '850hPa temperature anomalies larger than one standard deviation' (top panels) and '850hPa temperature negative anomalies larger than one standard deviation' (bottom panels).

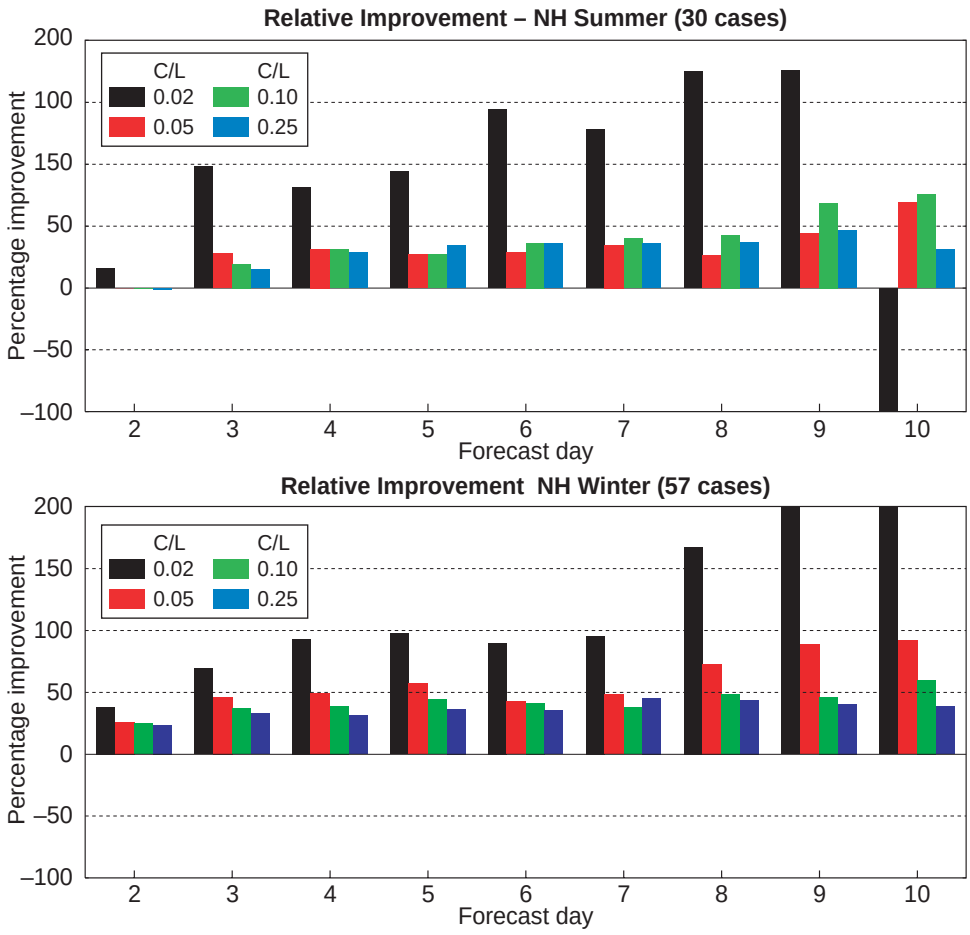

Figure 8 Relative Improvement index (RI) for the Value shown in Fig. 7 for summer (top) and winter (bottom) calculated for selected cost/loss ratios: C/L=0.02 (black), C/L=0.05 (red), C/L=0.10 (green) and C/L=0.25 (blue).

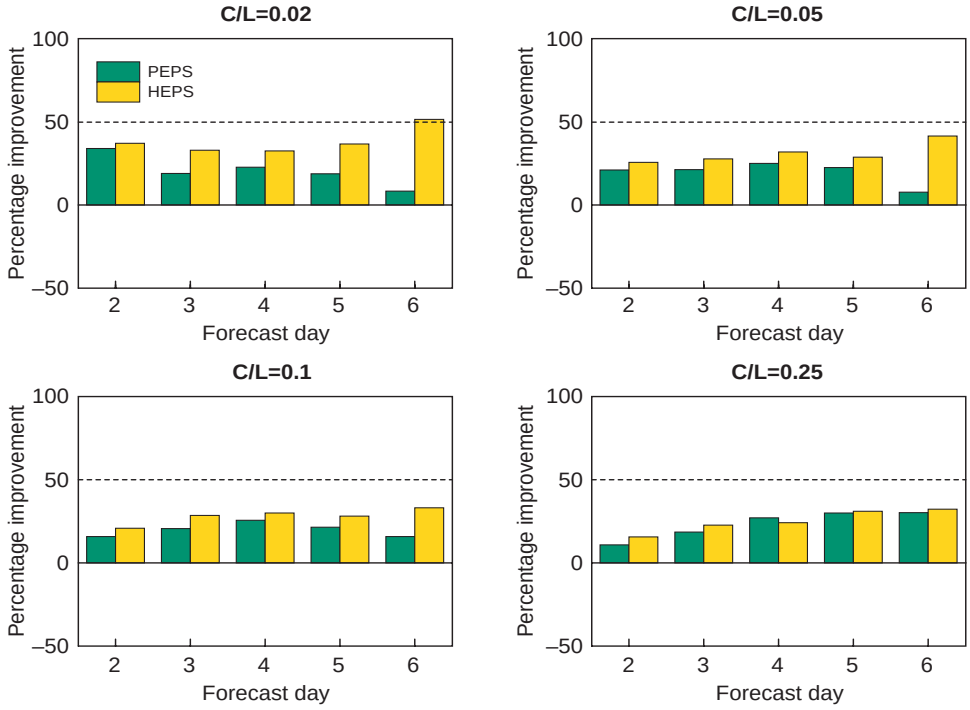

Figure 9 Relative Improvement index (RI) for the "Poor man's" ensemble PEPS (green) and the HEPS ensemble for winter (yellow) for selected cost/loss ratios: C/L=0.02 (top-left), C/L=0.05 (top-right), C/L=0.10 (bottom-left) and C/L=0.25 (bottom-right). These results have been computed for the 39 cases (out of the 57 considered so far) for which 500 hPa geopotential height fields for the other Centres were available (data for the 850hPa temperature field were not available, see text).

Potential economic value

The benefit of a forecast system will be different for different users. We illustrate this using the value diagnostic (V) derived from a simple decision-making model, the cost-loss model (*Richardson* 1998, 2000). V is a relative measure of the savings made by a forecast user: maximum value, V=1, will be obtained only with perfect knowledge of future weather, while V=0 indicates that the forecasts have no benefit over climatological information. Each user will have a different sensitivity to a particular weather event. This is represented in the model by the cost-loss ratio (C/L) which ranges between 0 and 1. Low values of C/L represent users with high sensitivity to adverse weather: the potential economic loss is high compared to the cost of taking protective action. The distribution of users' C/L is not well known, but is likely to be concentrated towards lower C/L.

Figure 7 shows V at day 6 for the two events. HEPS is consistently better than EPS for all users, with greatest benefit for those users with low cost-loss ratios. It can also be seen that the improvement relative to EPS(d-1) also varies with the user: the high-resolution benefits low cost-loss ratio users by one day or more.

Figure 8 shows the relative improvement index for V, calculated for a selection of cost-loss ratios. The variation in benefit with different users seen in Fig 7 is repeated at all forecast times. The RI for low cost-loss (0.02) is close to or exceeds 100% for forecast days 4–10. For larger cost-loss ratios, the RI is generally closer to 50%, similar to the RIs for the Brier Skill Score.

HEPS compared to "Poor man's" ensemble

An alternative approach to ensemble generation is provided by the so-called "poor man's" ensemble. One system proposed recently is the use of a small number of operational forecasts from different centres (*Ziehmann* 2000). Probabilities are obtained as in the EPS using the fraction of ensemble members that predict an event. Another option is to use a single deterministic integration and to generate probabilities using known error statistics of the deterministic model (*Atger* 1999). Here we consider a combination of the two methods. We use the operational high-resolution forecasts of ECMWF, the Met Office and DWD together with the lower resolution control forecasts available for ECMWF and the Met Office to construct a five-member ensemble of forecasts. Probabilities are generated by adding a Gaussian PDF to the ensemble-mean; the variance of the PDF is fixed, using the errors of the contributing models. This poor man's system will be referred to as PEPS. For comparison, the probabilities from the EPS and HEPS ensembles are similarly constructed, using the respective ensemble mean and a Gaussian PDF; however, for these systems, the variance of the PDF changes depending on the ensemble spread.

Because of the availability of data, results are only available for the 500hPa height and for just 39 of the 57 winter cases. Again we consider positive and negative anomalies of more than one standard deviation.

Figure 9 shows the relative improvement in V for PEPS and HEPS for the same cost-loss ratios as used in Fig 8. PEPS shows a consistent improvement over EPS. Further results (not shown) indicate that almost all of this benefit is a result of the higher resolution of the operational models used in PEPS. The increase in resolution of HEPS, although not as great as that of the operational models, is substantial enough to provide additional benefit over PEPS. The value of PEPS and HEPS is similar for larger values of C/L, but for smaller C/L the extra benefits of HEPS can be substantial.

It should be emphasised that the PEPS is only appropriate for basic single-parameter events where the forecast probabilities can be represented by a simple PDF. A major advantage of the ECMWF EPS is that probabilities for any combination of weather parameters can easily be extracted.

Equally easily, data for each EPS member can be input directly into a user's application model to provide a PDF of a user-specific parameter. Examples of such use of the EPS are ship routing (*Janssen* 2000), ice prediction (*Mureau et al.* 1997) and electricity demand (*Taylor and Buizza* 2000).

Summary

This work has shown that the new 80-km High-Resolution Ensemble Prediction System improves the estimate of the probability distribution function of forecast states. Results based on the Brier skill score of probabilistic predictions of moderate 850hPa temperature anomalies for the NH have indicated that the operational implementation of the new HEPS system has induced a gain in predictability of about 12 hours. Consideration of economic value confirms this overall level of improvement and also indicates substantially larger benefits for users with low cost-loss ratios. The new HEPS system outperforms a "poor man's" EPS containing higher resolution operational models.

The reader is referred to *Buizza & Hollingsworth* (2001a) and (2001b) for a discussion of the impact of the resolution increase on the prediction of severed storms. ❑

References

Atger, **F.**, 1999. The skill of ensemble prediction systems. *Mon. Wea. Rev.*, **127**, 1941-1953.

Barkmeijer, **J.**, **Buizza**, **R.**, & **Palmer**, **T.N.**, 1999: 3D-Var Hessian singular vectors and their potential use in the ECMWF Ensemble Prediction System. *Q.J.R. Meteor. Soc.*, **125**, 2333-2351.

Buizza, **R.**, & **Palmer**, **T.N.**, 1995: The singular-vector structure of the atmospheric general circulation. *J. Atmos. Sci.*, **52**, 1434-1456.

Buizza, **R.** & **Hollingsworth**, **A.**, 2001a: Severe Weather Prediction using the ECMWF EPS: The European Storms of December 1999. *ECMWF Newsletter No. 90 – Spring 2001.*

Buizza, **R.** & **Hollingsworth**, **A.**, 2001b: Storm prediction over Europe using the ECMWF Ensemble Prediction System. *Mon. Wea. Rev. submitted*.

Buizza, **R.**, **Petroliagis**, **T.**, **Palmer**, **T.N.**, **Barkmeijer**, **J.**, **Hamrud**, **M.**, **Hollingsworth**, **A.**, **Simmons**, **A.**, & **Wedi**, **N.**, 1998: Impact of model resolution and ensemble size on the performance of an ensemble prediction system. *Q.J.R. Meteorol. Soc.*, **124**, 1935-1960.

Buizza, **R.**, **Miller**, **M.**, & **Palmer**, **T.N.**, 1999: Stochastic simulation of model uncertainties. *Q.J.R. Meteorol. Soc.*, **125**, 2887-2908.

Buizza, **R.**, **Barkmeijer**, **J.**, **Palmer**, **T.N.**, & **Richardson**, **D.S.**, 2000: Current status and future developments of the ECMWF Ensemble Prediction System. *Meteorol. Appl.*, **7**, 163-175.

ECMWF, 1999: A Strategy for ECMWF 1999-2008. ECMWF, Shinfield Park, Reading, RG6-9AX, UK, pp. 16.

Janssen, **P.**, 2000: Potential benefits of ensemble prediction of waves. *ECMWF Newsletter No 86 – Winter 1999-2000.*

Molteni, **F.**, **Buizza**, **R.**, **Palmer**, **T.N.**, & **Petroliagis**, **T.**, 1996: The new ECMWF ensemble prediction system: methodology and validation. *Q.J.R. Meteorol. Soc.*, **122**, 73-119.

Mureau, **R.**, **Wessels**, **H.**, & **van Dorp**, **H.**, 1997: Skating on EPS. *ECMWF Newsletter No 74 – Winter 1996-97.*

Palmer, **T.N.**, **Molteni**, **F.**, **Mureau**, **R.**, **Buizza**, **R.**, **Chapelet**, **P.**, & **Tribbia**, **J.**, 1993: Ensemble prediction. Proceedings of the ECMWF Seminar on Validation of models over Europe: vol. I, ECMWF, Shinfield Park, Reading, RG2 9AX, UK.

Richardson, **D.S.**, 1998: Obtaining economic value for the EPS. ECMWF *Newsletter No 80 – Summer 1998.*

Buizza, **R.**, 2000: Skill and economic value of the ECMWF Ensemble Prediction System. *Q.J.R. Meteorol. Soc.*, **126**, 649-668.

Ziehmann, **C.**, 2000. Comparison of a single-model EPS with a multi-model ensemble consisting of a few operational models. *Tellus,* **52A**, 280-298.

R. Buizza, D.S. Richardson & T.N. Palmer

MARS on the Web: a virtual tour

MARS is ECMWF's archival system. It contains decades of observations and billions of meteorological fields. A year ago we endeavoured to give an easy access to all our users to this large amount of data using a standard web browser. This article describes the status of this project.

Writing an article about a web site is a quite difficult. It is not easy to describe with words something that is already a mixture of textual information, graphics and navigation hyperlinks. The difficulty comes from trying to describe a system that is inherently self-describing.

So the best way to learn about MARS on the Web is to actually use it! However, not every reader of this newsletter may be able to visit us. Therefore, the structure of this article tries to emulate navigation through the key components of the site[1].

But if you have a web browser handy and access to our Member States website meet us at http://wms.ecmwf.int/services/mars.

1 The Web is based on the paradigm of real sites containing virtual pages. You are about to visit a virtual site using a real page.

Let's start our tour . . .

First stop: Server activity

If you are already a MARS user, using either Metview or the MARS batch client, you will find this page very useful.

It displays the MARS activity in real time. You may follow the progress of your requests as they are processed by the MARS servers.

The information given, in particular the number of concurrent requests and the size of these requests (both in terms of fields and bytes) as well as the information about tape access, may help you understand where the delays lie in the processing of your requests.

By gaining the knowledge about the way MARS servers operate, you will be able to reorganise your requests in order to get the most out of the system.

Second stop: the MARS catalogue

Let's now move to the main part of the site, the catalogue describing the content of the archive. As you navigate through the catalogue, pages are created dynamically using the information stored in the Metadata database on top of which MARS is built. This means that the content of this catalogue is always accurate, and newly added data is immediately visible.

There are three ways you could use to start browsing the catalogue:

- If you are interested in recent data, you may start from the "Last operational archive" page. This page is automatically updated every night, according to what was archived by the operational suite. Any links from there will lead you to the corresponding page in the catalogue.

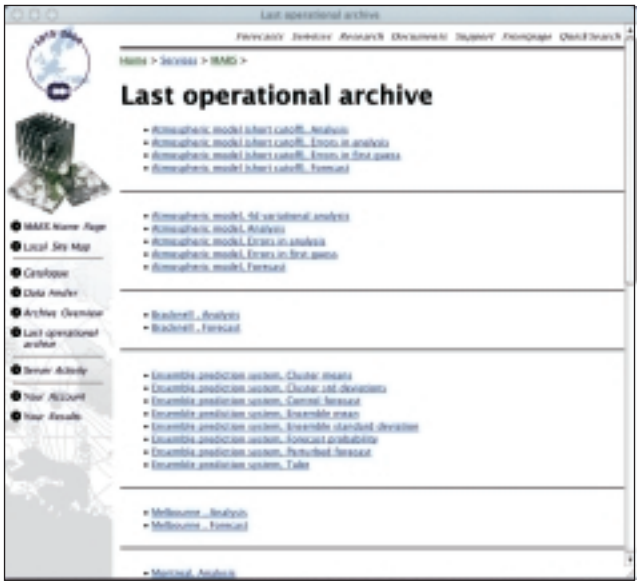

- If you are new to MARS, a manually edited page called "Archive overview" is an attempt to describe the archive in terms of data type and data source. The hierarchy shown here is not the same as the one in the catalogue. Following the links will send you into the catalogue, to the most recent data of that kind:

- Finally, if you want to reach any data archived in MARS, you should start from the top of the catalogue. Every single field of the billions archived is only a few clicks away from this page.

After cruising through the catalogue hierarchy (not shown here, otherwise this article would be too long), you will reach a page that represents an 'archive unit[2]'. It is a collection of related fields (a complete forecast, one month of analysis...). The concept of 'archive unit' is important for two reasons:

- All fields belonging to a unit are usually collocated on the same tape file, so retrievals from a unit are optimised.
- You presently cannot retrieve data from more than one unit (e.g. retrieve data from different months) in one go. The normal MARS client does not suffer from this limitation. This restriction will disappear in the near future.

Let's select a few fields in the lists, and choose an action. Let's start with "Plot the selection >>".

2 Also called "archive object" in earlier MARS design documents.

Plotting

The next page we will reach contains a description of the fields we have selected, together with three attributes that will be used to plot the fields. The default attributes are the ones we last used to do a similar plot.

We would like to change the geography used (map projection). By clicking on the corresponding thumbnail, we reach the following page:

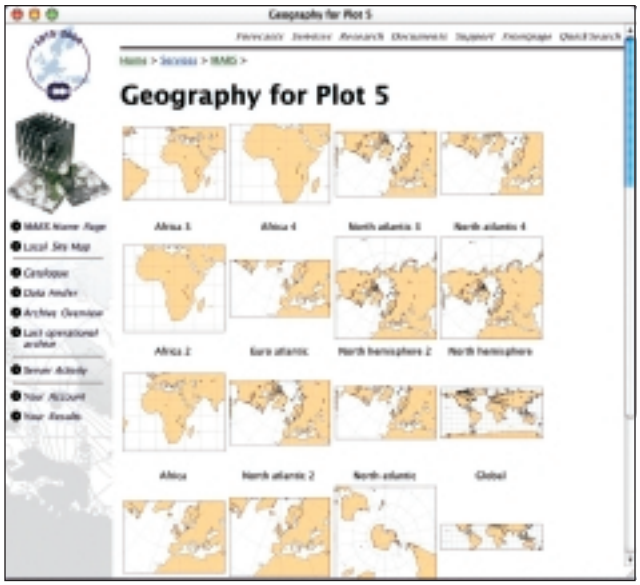

This page offers a selection of predefined geography. Let's choose "North Atlantic 3". The ability to define custom geographies is being currently developed.

We are now back to the previous page, with a new geography selected. Similarly we could select different settings for contouring and coastline drawings.

To start the task, simply click on "Now >>". A new page is displayed showing the status of the plot. The animated clock shows that the task is active. In this case the data has already been retrieved from the archive and the plot is currently being produced. This page update itself every 20 seconds, until the task is complete.

On completion, the image shows a set of fields, and the table contains the plot in various formats as well as the GRIB data that was retrieved from the archive.

Let's choose animation. In our example, seven days of temperatures at 500 hPa were requested.

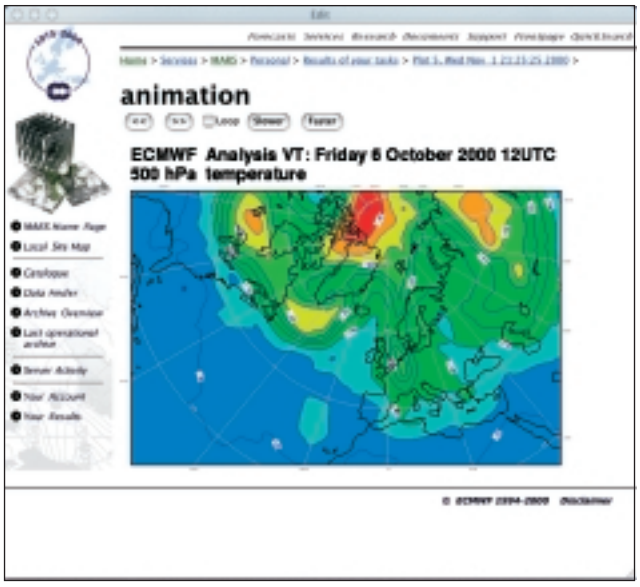

A detour: Your account

At the top of some of the previous pages, you may have noted a link to "Results of your tasks". This page holds the result of all your tasks for the last three days, as well as the status of your active ones. There is no need for you to wait for long retrievals. You could simply bookmark this page and come back to it from time to time.

If you click on "Personal", you will see various links to some pages containing information about your choices and preferences. This is where the last geography-contour and coastline attributes that you have selected are saved, so they could become the defaults for any future plots

From this page you will also be able to create some schedules, in order to have the system automatically retrieve or plot data for you. For example, a plot could be generated as soon as the data are archived by the operational suite, and be ready for you to consult when you arrive at work in the morning.

Data retrieval

Instead of plotting the data, we could have chosen to simply retrieve it. In this case, the attributes associated with that task are different. These attributes represent the post-processing facilities offered by MARS: representation changes, sub-area extraction, and interpolation to coarser resolutions.

Most of the fields in MARS are global (they cover the whole world) and are either on a Gaussian grid or in spherical harmonics, with a varying resolution throughout the archive history.

In this example, we have selected a different set of fields in the catalogue: the forecast accumulation of snow from the 15-year reanalysis.

Selecting the data, we move to the next page by selecting "Retrieve the selection >>".

The yellow note is a warning that the total number of fields requested is rather large (more that 20,000 fields).

Let's change the "grid" by clicking on the thumbnail. As for the geographies, we are presented with a choice of various grid intervals. Let's select a 1.5° by 1.5° grid.

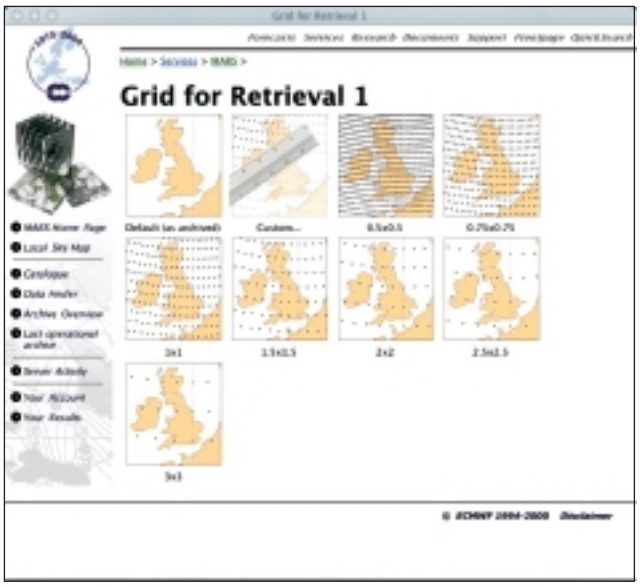

The next page allows us to define and name an area on the globe. This area will be added to the list of predefined areas for future use.

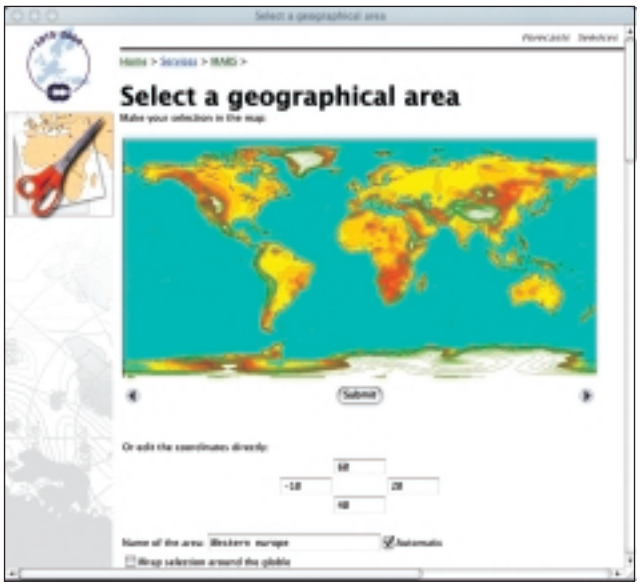

Back to the request page, let's change the settings for the sub-extraction. In this case, there are no suitable predefined areas. Let's choose "Custom . . .".

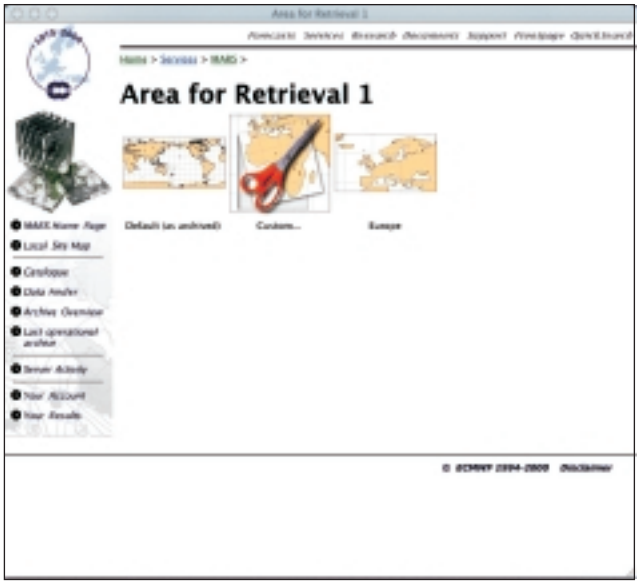

The post-processing attributes have now been specified. In this case, although the request is quite large in terms of fields, it will be very small in term of bytes as the area selected is small and the grid chosen is coarse.

We may choose to retrieve the data immediately, or retrieve them later using a schedule that was defined earlier (see Your Account) [3].

Other tasks

Not all combinations of parameters, levels or steps are available. Unfortunately, the way the catalogue presents the content of an archive unit (as a collection of lists) is not sufficient. Computing all the possible combinations is very time consuming and cannot be done on the fly.

Make a selection in the list and click on "Check the availability >>".

In this example (the output of the fifty members of the EPS) all parameters are available at all levels every 12 hours, but the geopotential and temperature are also available every six hours at 500 hPa and 850 hPa.

Another task is the evaluation of the "cost" of retrieving a set of fields from the archive. The cost is expressed in terms of number of fields, size in bytes and the number of tape mounts involved to fulfil the request.

In the future, if the ECMWF Data Services' ordering scheme is built on top of this system, real costs may be computed and presented to the potential buyer.

Third stop: the data finder

Finally, let's now visit the "Data finder". This finder is a small expert system built on top of a small knowledge base that contains information about all the fields archived by the operational suite and the reanalysis project. Any other fields, such as research experiments, are not visible here.

The idea behind the data finder is that different users may be looking for different things (or goals).

- One may want to study a particular period, and to know what parameters were archived at the time. Choosing a set of parameters to study, this user may then realise that they are available from the operational archive and the 15-year reanalysis, and decide to retrieve the data from the latter.
- Another may simply want to know when we started forecasting (and thus archiving) ozone related parameters.
- A third may want to know what is the period covered by the 15-year reanalysis.

The first user will start searching by specifying a time period, then a set of parameters and finally a data source. The second will start with a parameter and continue with a time period. The third will start with the data source.

Although the system could be interrogated on all possible attributes (date, step, level...), in any order, only the parameters date and data source are presently available through the interface.

3 Schedules are still under development.

Let's try. Our goal: a snow study for 1988. From this page we have three choices: select a parameter, a time period of a data source.

In our case, we are not interested in a specific data source, so let's start with selecting the year. This can be done by either typing the dates in the text fields, or by clicking the first and the last month of 1988 in the calendar.

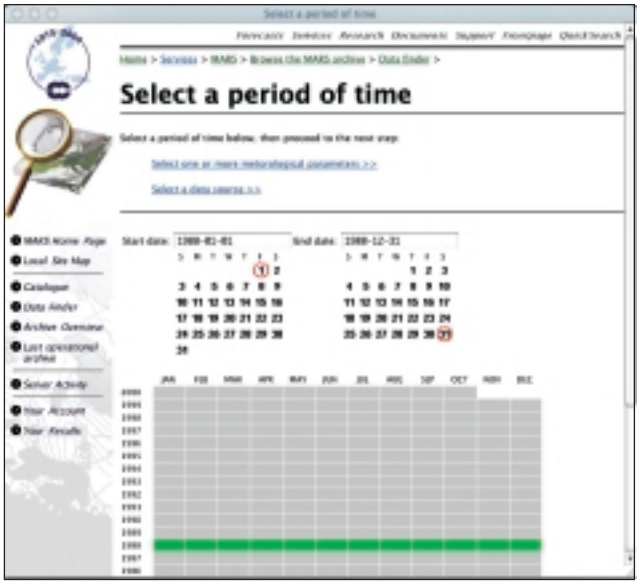

Moving to the choice of parameters, we are presented with the list of all the meteorological data that were produced during this year. We can filter this list to only show the parameters that we are interested in by typing "Snow" in the filter.

At this point we check all possible choices, and move to the next page where we are shown the various data sources where these fields are available for the given period.

Assuming we have chosen "Forecast accumulation" from the 15-year reanalysis, the last page will show our selection:

From there we can simply jump in the catalogue to view our selection. The yellow note warns us that the list of parameters only show four values (the four snow fields) out of 22 available. The fields can now be retrieved.

Thank you

We hope that you enjoyed the tour that more of 250 users have already taken during the few months that this system as been running.

Developing this site has taught us a lot about providing services through the means of standard web technologies. The learning curve was quite steep, but we have now a good framework on which we can build more facilities, in particular providing access to a wider audience through Data Services. ❑

Baudouin Raoult

New physics parameters in the MARS archive

The parametrization package in the IFS-model simulates a large number of parameters that are of direct interest to users. Examples are cloud cover, 10m wind, temperature and moisture at screen level, precipitation, radiative fluxes, etc.

Since IFS cycle 22R3 (introduced on 27 June 2000), a series of new parametrization-related parameters has been added to the post-processing and stored in MARS. They are also part of the ECMWF 40-year reanalysis (ERA40)[1].

The purpose of this short article is to describe the new fields and to give some background on how the parameters are calculated. So far the verification of the new parameters has been very limited, so they should be viewed as experimental at this stage. The new fields are all of the single-level type and are listed in Table 1.

Wind gusts at 10m height.

Wind gusts are reported in strong wind conditions, because the "extremes" are relevant for storm damage. The word "extreme" needs some specification, as how extreme the observed wind will be depends on the filtering characteristics of the anemometer system. A fast-response system will measure higher gusts than a very-heavy slowly responding anemometer. In order to get uniform observations, WMO defines a wind gust as the maximum of the wind averaged over three-second intervals. The requirement for persistence over a few seconds is relevant because only an extreme that lasts for a few seconds causes enough drag on structures to result in damage.

Table 1 New physics fields archived by MARS

Code	Name	Description	Units	Comments
49	10FG	10m wind gust	m s^{-1}	Max gust since last pp
50	LSPF	Stratiform precipitation fraction	s	Accumulated field
159	BLH	Boundary-layer height	m	
208	TSRC	Top net solar clear-sky radiation	W m^{-2}s	Accumulated field
209	TTRC	Top net thermal clear-sky radiation	W m^{-2}s	Accumulated field
210	SSRC	Surface net solar clear-sky radiation	W m^{-2}s	Accumulated field
211	STRC	Surface net thermal clear-sky radiation	W m^{-2}s	Accumulated field

[1] See http://wms.ecmwf.int/research/era/Archive_plan_TOC.html for a complete description of the ERA40-archive.

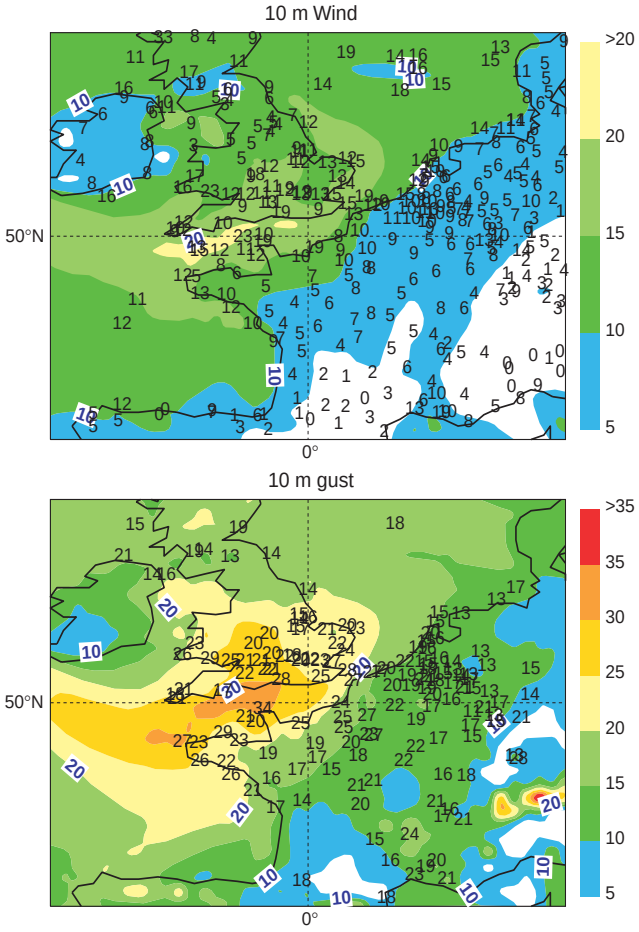

Figure 1 Wind at 10 m (top panel) and maximum gust over the previous 3 hours (bottom panel) for 8 December 2000 6 UTC. The contours are from a 42 hour forecast; the printed numbers are observations in m/s.

Because of the importance of extreme-wind forecasts, wind gusts are now parametrized and post-processed in the IFS model, and stored in the MARS archive. The principle is that the standard deviation of the horizontal wind is estimated and the difference between the gust and mean wind is made proportional to this standard deviation on the basis of universal turbulence spectra. Wind standard deviations and spectra are based on standard Monin-Obukhov similarity, where horizontal wind fluctuations are characterised by surface friction, surface buoyancy flux, and boundary-layer depth (see *Beljaars* (1987) for a description of the theory and for comparisons with observations). From the controlling parameters it is clear that the effects of surface friction (through surface roughness) and stability are captured. However, the approach might be less adequate for gusts in baroclinic situations and gusts due to strong convective events.

Figure 1 shows an example of a strong-wind situation, with the mean wind shown in the upper panel and the gusts in the lower panel; the printed numbers show the mean wind and gusts observed from the SYNOP stations. It should be noted that the mean wind is an instantaneous field whereas the gust field represents the maximum gust that has occurred since the last post-processing time (the previous three-hour interval in this case).

The gust field has the expected characteristics: the gusts are less affected by coastlines than the mean winds are, and the gusts are substantially higher than the mean. The extremes in the south of England and over the coast of Brittany and Normandy are reasonably well captured, but more inland in France the model's gusts are too low. As can be expected from observations, gusts vary substantially from one location to another, and so a big sample is needed in order to get a good impression of possible biases.

Stratiform precipitation fraction.

The model changes for IFS cycle CY21R4, reported in the ECMWF Newsletter 87, include a novel treatment of stratiform (or large-scale) precipitation. These include the description of precipitation by separate cloudy and clear-sky fluxes and, more importantly, a model grid box is allowed to be only partly covered by precipitation. This might appear conceptually difficult, especially when associating subgrid coverage with the words large-scale precipitation. However, the possible determination of subgrid coverage from what is better termed stratiform precipitation is a direct consequence of allowing for partial cloud cover, a very familiar concept. If the sky is only partly covered by clouds, precipitation falling out of them will naturally only cover part of a grid box.

In the new precipitation treatment of the model, the determination of the stratiform precipitation fraction forms an integral part of the model formulation. It is calculated by tracking the coverage of both cloudy and clear-sky precipitation from one model level to the next (for details see *Jakob and Klein*, 2000). It is thought that the coverage of precipitation at the ground might be a useful addition to the available model products. Therefore, the stratiform precipitation fraction at the surface has been added to the standard post-processed model parameters.

A difficult decision to make is whether the stratiform precipitation fraction should be consistent with the cloud fraction (and, therefore, be post-processed as an instantaneous value) or with the stratiform (large-scale) precipitation, which requires post-processing as an accumulated field to provide a true average over the post-processing period. Currently the second option is chosen.

There are a number of potential applications for stratiform precipitation fraction, although not all of them will be achievable with the currently post-processed time-accumulated values. The most obvious of these applications is the estimation of the mean local rainfall rate, defined as the grid-mean stratiform precipitation divided by the precipitation fraction, assuming a steady state over the accumulation (averaging) interval. Other, more complex applications, such as the estimation of a spatial rainfall distribution function, appear feasible but will require substantial further research. The main reason, however, to post-process the stratiform precipitation fraction at this stage is that it is a verifiable quantity. Verification would require the use of either rain radar observations or data gathered by high-resolution rain-gauge networks.

To provide an example of the new field, Figure 2 shows the stratiform precipitation fraction (top panel), the stratiform (large-scale) precipitation rate (middle panel) and the

local stratiform precipitation rate (bottom panel) from the operational 42-hour to 48-hour forecast initialised on 15 July 2000. All values shown represent true six-hour averages valid between 6 and 12 UTC 17 July 2000. It is interesting to note that, while the precipitation fraction frequently reaches its maximum value of one, in many areas it is smaller than that. The consequences for the local precipitation rate are evident when comparing the middle and lower panel. While, in the area of high precipitation, the fraction grid-mean and local precipitation rates are almost identical, the local precipitation rate (for instance, over southern Italy) is substantially higher than the grid-mean. In fact, judging by the grid-mean values, not much precipitation at all would have been expected in that area, while the local rain rate, which according to the precipitation fraction will fall over less than 30% of a grid box, reaches values of more than 5 mm/day.

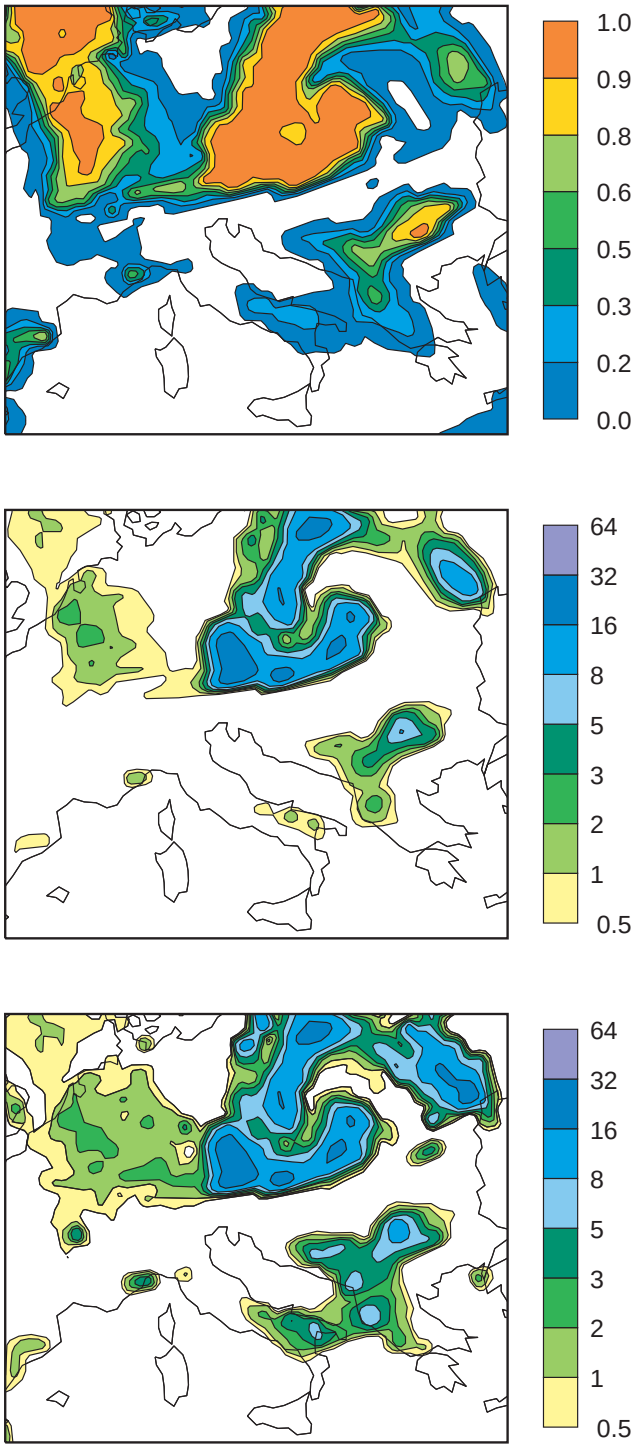

Figure 2 42 to 48-hour forecast of stratiform precipitation fraction (top), grid-mean stratiform precipitation rate (middle), and local stratiform precipitation rate (bottom). The initial time is 12 UTC 15 July 2000. Units for precipitation are mm/day.

Boundary-layer height

Boundary-layer height is an important parameter in the turbulence parametrization of the IFS model, since it determines the scaling of diffusion coefficients in the mixed layer and in the boundary-layer-top entrainment (*Beljaars and Viterbo*, 1999). Boundary-layer height is also important for applications in air-pollution transport modelling, because it determines the height over which pollution is mixed if the pollutant release takes place in the boundary layer (*Gryning et al.*, 1997). In the case of tall stacks, it is also possible that the release may take place above the (stable) boundary layer. So the precise position of the boundary-layer top with respect to the release height is important because it determines whether the pollutant will be mixed down to the surface by boundary-layer turbulence.

In order to determine the boundary-layer height in the IFS model, a diagnostic routine has been added to the parametrization package. It is based on the parcel-lifting method proposed by *Troen and Mahrt* (1986). The parcel is lifted from the surface layer up to the level where a critical bulk Richardson number is reached (the boundary-layer height). The advantage of this method is that it is robust and that it gives an answer for stable as well unstable situations. Consistent with the turbulence scheme, the parcel-lifting method uses dry static energy as a conserved variable and, therefore, the boundary-layer top will be near cloud base in the case of a cloud-topped boundary layer. The quality of the resulting estimate obviously depends on the realism of the wind and temperature profiles.

Figure 3 shows daytime and night-time boundary-layer heights for a summer situation over Europe. The diurnal cycle is very pronounced, with deep daytime mixed layers and shallow boundary layers at night. The experience so far with this new model product is limited, but the behaviour of boundary-layer height looks very realistic. An example of a diurnal cycle in the Netherlands is shown in Figure 4, in which the model output (with a high time resolution) is compared with profiler data.

Clear-sky radiative fluxes

Since the pioneering study of *Cess and Potter* (1987) and *Ramanathan et al.* (1989), so-called "cloud forcing" has become a popular diagnostic for assessing the role of clouds in climate sensitivity studies. The building blocks for cloud forcing are the usual top-of-the-atmosphere radiative fluxes (including the effects of clouds) and the radiative fluxes in clear-sky conditions, i.e. assuming the clouds to be completely inactive for both the long-wave and short-wave radiation

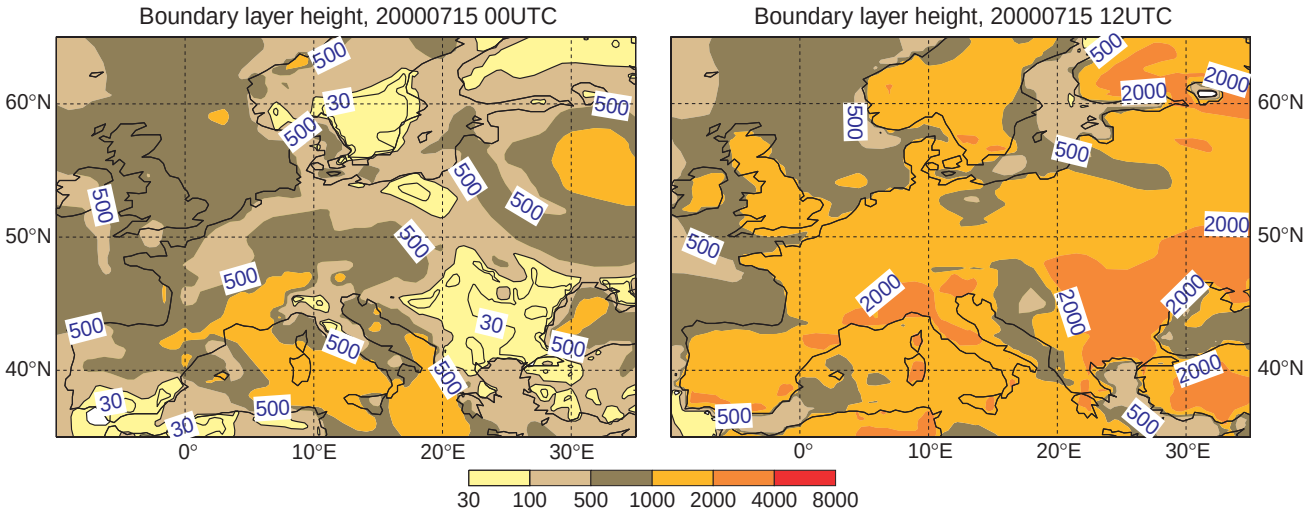

Figure 3 Boundary-layer height from an operational 36 and 48-hour forecast verifying at 00 UTC 15 July 2000 (left panel) and 12 UTC 15 July 2000 (right panel), respectively.

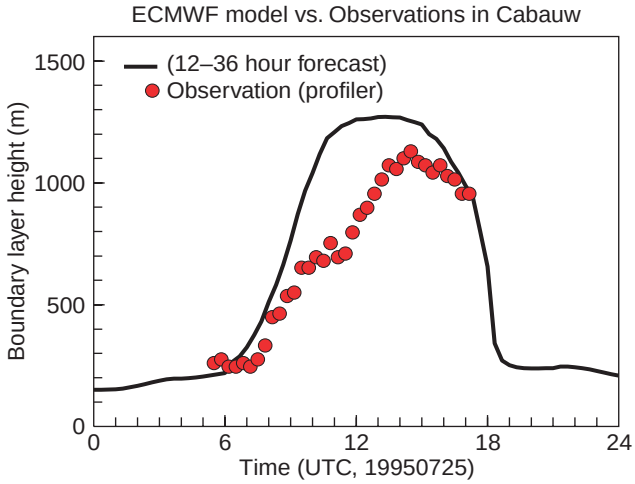

Figure 4 Diurnal evolution of the boundary-layer height for Cabauw in The Netherlands compared with profiler data for 25 July 1995 (data provided by Henk Klein Baltink, KNMI).

transfer. The cloud forcing, simply computed as the difference between the total and the clear-sky fluxes, represents the impact of clouds on the flux (either long-wave or short-wave) at the top of the atmosphere or at the surface. The ratio of the short-wave cloud forcing at the surface and the short-wave cloud forcing at the top of the atmosphere has recently been at the centre of the discussion about anomalous short-wave absorption (*Cess et al.*, 1995; *Imre et al.*, 1996).

The radiation scheme within the ECMWF model has long been able to provide these clear-sky fluxes, but the information provided had, up until now, never been part of the operational archiving. However, these clear-sky fluxes have been available since the introduction of IFS cycle 22R3. Figure 5 presents the long-wave and short-wave cloud forcing terms over the globe averaged over all operational 24-hour forecasts for July 2000, as seen from the top of the atmosphere. ❑

References

Beljaars, A.C.M., 1987: The influence of sampling and filtering on measured wind gusts, *J. Atmos. Ocean. Technol.*, **4**, 613-626.

Beljaars, A.C.M. and **P. Viterbo**, 1999: 'The role of the boundary layer in a numerical weather prediction mode'. In Clear and cloudy boundary layers, Eds. A.A.M. Holtslag and P.G. Duynkerke, North Holland Publishers.

Cess, R.D., and **G.L. Potter**, 1987: Exploratory studies of cloud radiative forcing with a general circulation model. *Tellus*, **39A**, 460-473.

Cess, R.D., M.H. Zhang, P. Minnis, L. Corsetti, E.G. Dutton, B.W. Forgan, D.P. Garber, W.L. Gates, J.J. Hack, E.F. Harrisson, X. Jing, J.T. Kiehl, C.N. Long, J.-J. Morcrette, G.L. Potter, V. Ramanathan, B. Subasilar, C.H. Whitlock, D.F. Young and **Y. Zhou**, 1995: Absorption of solar radiation by clouds: Observations versus models. *Science*, **267**, 496-499.

Gryning, S.-E., F. Beyrich and **E. Batchvarova**, 1997: The determination of mixing height - Current progress and problems, EUROSAP workshop proceedings, 1-3 October 1997, Riso National Laboratories, Roskilde, Denmark.

Imre, D.G., E.H. Abramson, and **P.H. Daum**, 1996: Quantifying cloud-induced short-wave absorption: An examination of uncertainties and of recent arguments for large-scale excess absorption, *J. Appl. Meteor.*, **35**, 1991-2010.

Jakob, C. and **S.A. Klein**, 2000: A parametrization of the effects of cloud and precipitation overlap for use in general-circulation models, *Q.J.R. Meteorol. Soc.*, **126**, 2525-2544.

Ramanathan, V., R.D. Cess, E.F. Harrison, P. Minnis, B.R. Barkstrom, E. Ahmad and **D. Hartmann**, 1989: Cloud-radiative forcing and climate: Results from the Earth Radiation Budget Experiment. *Science*, **243**, 57-63.

Troen, I. and **L. Mahrt**, 1986: A simple model of the atmospheric boundary layer; sensitivity to surface evaporation, Boundary-Layer *Meteorol.*, **37**, 129-148.

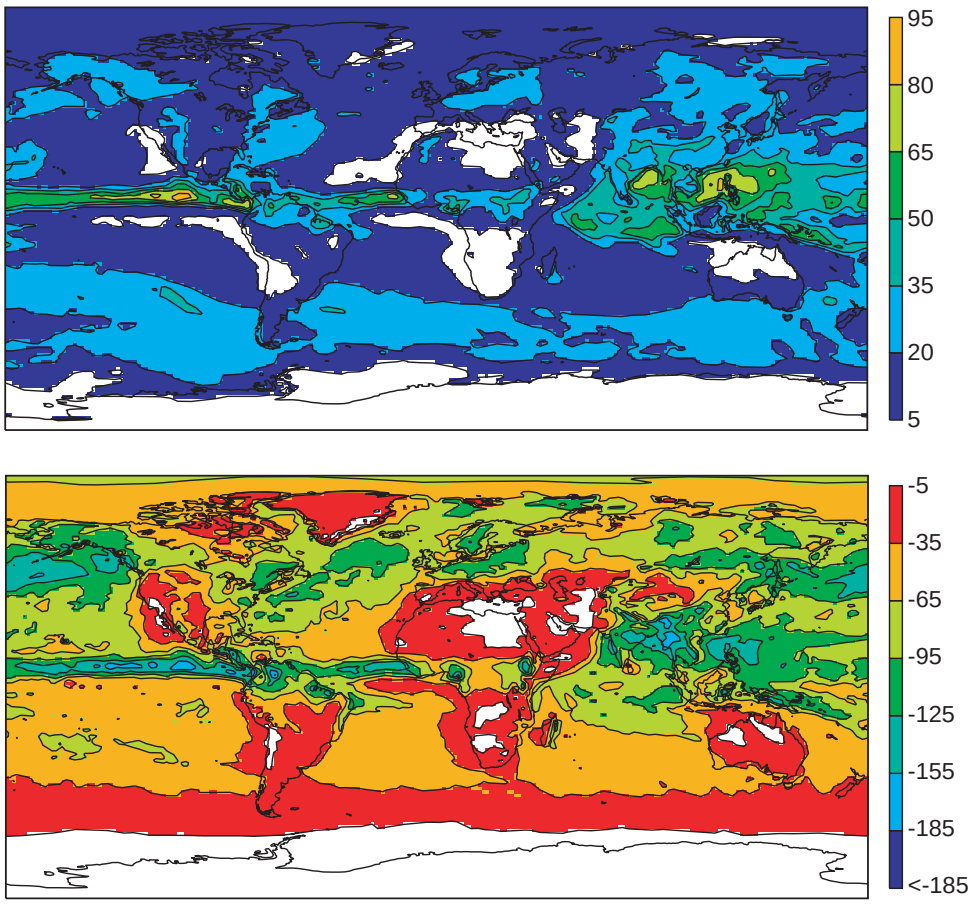

Figure 5 The long-wave (top panel) and short-wave (bottom panel) cloud radiative forcing (the total minus the clear-sky radiation) at the top of the atmosphere averaged over all operational 24-hour forecasts of July 2000.

Anton Beljaars, Christian Jakob and Jean-Jacques Morcrette

ECMWF Calendar 2001

2 – 11 Apr	**Met NM** – *Numerical methods, adiabatic formulation of models*	
23 – 27 Apr	**Met PR** – *Predictability, diagnostics & seasonal forecasting*	
30 Apr – 11 May	**Met PA** – *Parametrization of diabatic processes*	
14 – 23 May	**Met DA** – *Data assimilation & use of satellite data*	
Apr 2 – 3	**Security Representatives meeting**	
May 3 – 4	**Computer Representatives meeting**	
May 22 – 23	**Policy Advisory Committee**	*14th*
May 29 – 30	**Finance Committee**	*65th*
June 18 – 19	**Medium-Range Forecasts' Users Meeting**	
June 20 – 21	**Seasonal Forecasts' Users Meeting**	
June 28 – 29	**Council**	*54th*
July 2 – 4	**Workshop** – *Ocean Wave Forecasting*	
Sept 3 – 7	**Seminar** – *Key issues in the parametrization of subgrid-scale processes*	
Oct 1 – 3	**Scientific Advisory Committee**	*30th*
Oct 8 – 10	**Technical Advisory Committee**	*30th*
Oct 15 – 16	**Finance Committee**	*66th*
Oct 18 – 19	**Policy Advisory Committee**	*15th*
Nov 5 – 9	**Workshop** – *Reanalysis*	
Nov 12 – 16	**Eighth ECMWF Workshop on Meteorological Operational Systems**	
Dec 10 – 11	**Council**	*55th*

Table of Member State and Cooperating State TAC Representatives, Computing Representatives and Meteorological Contact Points

Member State	TAC Representative	Comp. Representative	Met.Contact Points
Belgium	Dr. W. Struijlaert	Mrs. L. Frappez	Dr. J. Nemeghaire
Denmark	Mr. L. Laursen	Mr. N. Olsen	Mr. G. Larsen
Germany	Prof. G.-R. Hoffmann	Dr. E. Krenzien	Mr. D. Meyer
Spain	Mr. T. Garcia Meras	Mr. E. Monreal Franco	Mr. F. Jimenez
France	Mr. B. Strauss	Mrs. M. Pithon	Mr. J. Clochard
Greece	Dr. G. Sakellaridis	Mr. A. Emmanouil	Mr. I. Papageorgiou Mr. P. Xirakis
Ireland	Mr. J. Logue	Mr. P. Halton	Mr. M. R. Walsh
Italy	Dr. S. Pasquini	Dr. G. Tarantino	Dr. G. Maresca
Netherlands	Mr. A.R. Moene	Mr. H. de Vries	Mr. G. Haytink
Norway	Mr. J. Sunde	Ms. R. Rudsar	Mr. P. Evensen
Austria	Dr. G. Wihl	Dr. G. Wihl	Dr. H. Gmoser
Portugal	Mrs. I. Barros Ferreira	Mrs. M.C. Pereira Santos Mr. J.C. Monteiro	Mr. F. Prates
Switzerland	Mr. P. Müller	Mrs. C. Raeber	Mr. R. Mühlebach
Finland	Mrs. K. Soini	Mr. T. Hopeakoski	Mr. P. Nurmi
Sweden	Mr. I. Karro	Mr. R. Urrutia	Mr. O. Åkesson
Turkey	Dr. M. Demirtas	Mr. N. Yaman	Dr. S. Sari
United Kingdom	Dr. A. Dickinson	Dr. A. Dickinson	Mr. A. Radford

Cooperating States	TAC Representative	Comp. Representative	Met.Contact Points
Croatia	**	Mr. M. Malović	Mr. D. Glasnović
Hungary	**	Ms. G. Duska	Mr. I. Ihasz
Iceland	Dr. M.Jonsson		Mr. G. Hafsteinsson
Slovenia	**	Mr. M. Kozelj	Mr. B. Gregorčič

** The Cooperating States: Croatia, Hungary and Slovenia are represented by the Chairman of the ACCS (Dr. Branko Gelo) who attends the TAC sessions as an observer.

ECMWF publications

Technical Memoranda:

311 **H. Järvinen**: Temporal evolution of innovation and residual statistics in the ECMWF variational data assimilation systems, *October 2000*

313 **F. Bouttier** and **G. Kelly**: Observing systems experiments in the ECMWF 4D-Var data assimilation system, *February 2001*

315 **J-R. Bidlot**, **D.J. Holmes**, **P.A. Wittmann**, **R. Lalbeharry** and **H.S. Chen**: Intercomparison of the performance of operational ocean wave forecasting systems with buoy data, *September 2000*

319 **M.J.P. Cullen**: Alternative implementations of the semi-Lagrangian semi-implicit schemes in the ECMWF model, *October 2000*

320 **J. Segschneider**, **D.L.T. Anderson**, **J. Vialard**, **M. Balmaseda**, **T.N. Stockdale**, **A. Troccoli** and **K. Haines**: Initialisation of seasonal forecasts assimilating sea-level and temperature observations, *December 2000*

325 **C. Cardinali**: EUCOS impact study, *December 2000*

327 **J-J. Morcrette**: Assessment of the ECMWF model cloudiness and surface radiation fields at the ARM-SGP site, *January 2001*

330 **Bauer**, **P**: Rain detection over land surfaces using passive microwave satellite data, *January 2001*

331 **Bouttier**, **F.** The use of profiler data at ECMWF *January 2001*

Workshop Proceedings

ECMWF Workshop on Developments in numerical methods for very-high-resolution global models, *5-7 June 2000.*